Clim. Past Discuss., 9, 6515–6549, 2013
www.clim-past-discuss.net/9/6515/2013/
doi:10.5194/cpd-9-6515-2013

Climate of the Past
Discussions
Open Access

Model-data comparison and data assimilation of mid-Holocene Arctic sea-ice concentration

F. Klein[1], H. Goosse[1], A. Mairesse[1], and A. de Vernal[2]

[1]Université catholique de Louvain, Earth and Life Institute, Georges Lemaître Centre for Earth and Climate Research, Place Louis Pasteur, 3, 1348 Louvain-la-Neuve, Belgium
[2]GEOTOP, Université du Québec à Montréal, P.O. Box 8888, succursale "centre ville" Montréal, Qc, H3C 3P8 Canada

Received: 15 November 2013 – Accepted: 29 November 2013
– Published: 10 December 2013

Correspondence to: F. Klein (francois.klein@uclouvain.be)

Published by Copernicus Publications on behalf of the European Geosciences Union.

Abstract

The consistency between a new quantitative reconstruction of Arctic sea-ice concentration based on dinocyst assemblages and the results of climate models has been investigated for the mid-Holocene. The comparison shows that the simulated sea-ice changes are weaker and spatially more homogeneous than the recorded ones. Furthermore, although the model-data agreement is relatively good in some regions such as the Labrador Sea, the skill of the models at local scale is low. The response of the models follows mainly the increase in summer insolation at large scale. This is modulated by changes in atmospheric circulation leading to differences between regions in the models that are albeit smaller than in the reconstruction. Performing simulations with data assimilation using the model LOVECLIM amplifies those regional differences, mainly through a reduction of the southward winds in the Barents Sea and an increase in the westerly winds in the Canadian Basin of the Arctic. This leads to an increase in the ice concentration in the Barents and Chukchi Seas and a better agreement with the reconstructions. This underlines the potential role of atmospheric circulation to explain the reconstructed changes during the Holocene.

1 Introduction

Sea-ice is a key element of the global climate system. First, it enhances climate response at high latitudes of the Northern Hemisphere as it is involved in various feedbacks, in particular the classical ice albedo feedback (Holland and Bitz, 2003; Serreze et al., 2009; Screen and Simmonds, 2010; Stroeve et al., 2011). Second, sea-ice plays a role in deep water formation through brine rejection which is a crucial driver of the global thermohaline circulation (Lohmann and Gerdes, 1998; Goosse and Fichefet, 1999). Third, it modifies the exchanges of heat and gases between the atmosphere and polar oceans because of its insulation properties (Ebert and Curry, 1993). Consequently, changes in Arctic sea-ice cover and thickness influence the atmospheric and

CPD
9, 6515–6549, 2013

hydrographic conditions at high latitudes, which may in turn have an impact on the European and the North-American climate (e.g. Serreze et al., 2007; Francis and Vavrus, 2012).

The processes involved in the sea-ice behavior are complex, which explains why climate models still have clear biases in simulating sea-ice for present-day conditions (Stroeve et al., 2012; Massonnet et al., 2012). It is thus important to improve our understanding of sea-ice and its representation in climate models, especially in the current context of a decreased Arctic sea-ice cover and thickness over the past few decades (Serreze et al., 2007; Stroeve et al., 2011), likely related to anthropogenic climate change (e.g. Notz and Marotzke, 2012).

The analysis of past sea-ice fluctuations provides an interesting complement to the study of the last decades, in particular the ones focusing on the Holocene (the current interglacial) as the boundary conditions of the climate system were roughly similar to the present ones (Wanner et al., 2008). In the absence of direct instrumental measures, this can be achieved by two complementary approaches, proxy-based reconstructions (e.g. Funder et al., 2011; Müller et al., 2012) and modelling (e.g. Goosse et al., 2013; Berger et al., 2013). This allows, amongst others, to contextualize the recent climate changes, to validate climate models results, and to improve the physical understanding of the system (Zhang et al., 2010; Braconnot et al., 2012).

Here we will focus on the mid-Holocene (6 ka, hereafter MH) as it is a classical period that is reasonably well documented as much in terms of proxy data (see Sect. 3.1) as in terms of models results since it is a standard target for the Paleoclimate Model Intercomparison Project (PMIP, e.g. Braconnot et al., 2007). The MH coincides with the end of a warm period in the Arctic that started about 9 ka (Sundqvist et al., 2010) due to a high orbitally-driven summer insolation. Insolation has its maximum at around 11 ka (Berger, 1978) but the warmest conditions have been asynchronous across the Arctic due to the effect of the lingering Laurentide Ice Sheet (Kaufman et al., 2004; Renssen et al., 2009). At 6 ka, some regions were thus already experiencing a cooling

CPD
9, 6515–6549, 2013

(for instance Alaska) while others were still close to their maximum temperature (like northeast Canada) (Kaufman et al., 2004).

Although most Arctic proxies support lower sea-ice conditions during the MH as compared to the entire Holocene, the recorded changes are not homogeneous between the different regions (see Sect. 3.1). In addition to modifications in the oceanic and atmospheric circulations or to the influence of the remnant Laurentide Ice Sheet that could have an impact at a large scale, complex local topography can be responsible for a high heterogeneous response on small spatial scales. This is particularly the case in the Canadian Arctic Archipelago (CAA) with its complicated disposition of narrow straits, where proxy records display contrasted signals for nearby locations (e.g. Vare et al., 2009; Atkinson, 2009). Furthermore, the uncertainties related to the interpretation of proxies or to their dating can also explain some of the discrepancies (Polyak et al., 2010; Sundqvist et al., 2010).

In qualitative agreement with data, models simulate less sea-ice extent in summer during the MH as compared to the pre-industrial (PI) conditions, following the higher summer insolation (Berger et al., 2013; Goosse et al., 2013). However, no quantitative estimate of the agreement exists up to now given the lack of a consistent quantitative sea-ice reconstruction covering the Arctic. In this context, this paper aims at comparing the MH sea-ice concentration simulated by the model of intermediate complexity LOVECLIM and by general circulation models (GCMs) with a new quantitative reconstruction of Arctic sea-ice concentration based on dinocyst assemblages (de Vernal et al., 2013). This model-data comparison is intended first to estimate if climate models are able to reproduce the spatial pattern deduced from proxy records. In a second step, a simulation with data assimilation is performed with the climate model LOVECLIM. The impact of this additional constraint improves by construction the consistency between the models results and the reconstructions. This allows investigating in more details the processes governing sea-ice conditions at 6 ka and analysing the potential origin of the biases seen in the simulations without data assimilation.

CPD
9, 6515–6549, 2013

The models selected, the experimental design and the proxy reconstruction based on dinocyst assemblages are presented in Sect. 2. Section 3 starts with a short description of the observed sea-ice changes. It is followed by an analysis of the results of the simulations without data assimilation and finally of the simulation with data assimilation. Conclusions are presented in Sect. 4.

2 Methodology

2.1 Models description

Experiments have been performed with the three-dimensional Earth climate model of intermediate complexity LOVECLIM version 1.2 (Goosse et al., 2010). It includes a representation of the atmosphere, ocean, sea-ice and land surface including vegetation. The atmospheric component is ECBilt2 (Opsteegh et al., 1998), a quasi-geostrophic spectral model with T21 horizontal resolution (corresponding to $5.6^{\circ} \times 5.6^{\circ}$ latitude-longitude) and 3 vertical levels in addition to the surface. Ocean and sea-ice are simulated by CLIO3 (Goosse and Fichefet, 1999), which is a general circulation model coupled to a comprehensive thermodynamic-dynamic sea-ice model. Its horizontal resolution is of 3° by 3° and the ocean is divided into 20 unevenly spaced vertical levels. LOVECLIM also contains the vegetation model VECODE (Brovkin et al., 2002), that takes into account the distibution of 3 different land covers (deserts, grasses and forests) using the same resolution as ECBilt2. Due to its coarse resolution and to simplifications introduced in the representation of some atmospheric processes, LOVECLIM is much faster than the more sophisticated coupled climate models. It allows to produce the large amount of simulations required for the data assimilation process (see Sect. 2.2). In this study, two different 6 ka LOVECLIM simulations are examined: LOVECLIM without assimilation (referred as LOVECLIM no assim) and LOVECLIM with sea-ice data assimilation (LOVECLIM assim SIC).

CPD
9, 6515–6549, 2013

In addition to LOVECLIM simulations, MH experiments performed with GCMs following the framework of the third phase of the Paleoclimate Modelling Intercomparison Project (PMIP3, Otto-Bliesner et al., 2009), referred as *midHolocene*, are analyzed. The simulations from which the PI reference values have been obtained cover the period 1850–2000 and are referred as *historical* in the fifth phase of the Coupled Model Intercomparison Project (CMIP5, Taylor et al., 2012). The GCMs selected here (Table 1) are the ones for which the variables of interest for our diagnostics were available at the time of the analysis.

2.2 Data assimilation method

LOVECLIM results have been constrained to follow a proxy-based sea-ice reconstruction through a process of assimilation, using a particle filter with re-sampling (van Leeuwen, 2009; Dubinkina et al., 2011), in the same way as in several recent studies (e.g. Goosse et al., 2012; Mathiot et al., 2013; Mairesse et al., 2013). First, an ensemble of 96 simulations (called particles) is initialized from slightly different sea surface temperature for each particles, allowing different time developments. After 1 yr of simulation, the likelihood of each particle is computed from the difference between the proxy-based reconstructed and the simulated sea-ice concentration. The particles too distant from the reconstruction are abandoned whereas the ones close enough are kept as a basis for the next year simulation. In order to maintain a constant number of particles until the end of the simulated period, a resampling function of the particles likelihood is conducted annually. The sea surface temperature of the copies is once more perturbed to obtain different time developments for the following year, and the whole procedure is repeated sequentially every year until the end of the simulation, here 400 yr.

CPD
9, 6515–6549, 2013

2.3 Proxy-based sea-ice reconstruction

The MH proxy-based sea-ice reconstruction used to evaluate models performance and to constrain LOVECLIM simulations is derived from cysts produced by dinoflagellates (dinocyst). The dinocyst distribution in Arctic and sub-Arctic seas is indeed controlled by several environmental parameters including productivity, salinity, temperature and most importantly sea-ice (de Vernal and Rochon, 2011). The dataset is based on the dinocyst content of 18 cores collected in the North Atlantic and Arctic Oceans (Table 2 and Fig. 1). Sea-ice reconstruction is expressed in terms of annual mean concentration (in %) and is associated with a standard error of ±11 % (de Vernal et al., 2013). This value is used as the estimate of the reconstruction uncertainty for the evaluation of the likelihood in the experiment with data assimilation.

The proxy records include variability at (multi-)centennial time scale that could not be reproduced in the time-slice experiments performed following the PMIP protocol. Therefore, we consider the MH as a period of 1 kyr, i.e. 6 ± 0.5 ka, which limits the contribution of internal variability and non-orbital forcings. The choice of such an interval length also allows neglecting the potential biases related to dating uncertainties.

The model-data comparison and the data assimilation are performed using anomalies considering the PI conditions (1850–1900 yr AD) as reference period. We have preferred this option rather than using recent observed sea-ice cover, since comparing sea-ice conditions inferred from dinocyst content with satellite data would have lead to additional uncertainties. Furthermore, the recent period is far from being adequate for calculating anomalies since it presents rapid changes characterized by a significant decrease in sea-ice (e.g. Stroeve et al., 2011). Unfortunately, many of the available reconstructed time series used here are not continuous up to 1900. We have thus decided to reconstruct the reference dataset by computing a linear interpolation of those time series up to the period 1850–1900 AD. To avoid extrapolating over too long periods, the proxy records ending before 2 ka have been discarded from our analysis.

CPD
9, 6515–6549, 2013

2.4 Experimental design

All the MH simulations represent equilibrium conditions corresponding to 6 ka. They use the orbital forcing following Berger (1978). The changes in greenhouse gases concentration are taken from Flückiger et al. (2002) for LOVECLIM simulations, which is slightly different of the ones used in the framework of CMIP5/PMIP3 (http://pmip3.lsce.ipsl.fr/). As in Mathiot et al. (2013) and Mairesse et al. (2013), LOVECLIM simulations also consider slight changes in ice sheets topography and surface albedo following the reconstruction of Peltier (2004), as well as in freshwater fluxes from Antarctic ice sheet melting according to Pollard and DeConto (2009) results. This represents a small difference as compared to the CMIP5/PMIP3 protocol as the latter prescribes present-day ice sheet topography and no change in freshwater fluxes at 6 ka with respect to present. However, this has virtually no effect on results.

For the reference period corresponding to PI values, we have averaged all the results from available members for each GCM and from a set of experiments with LOVECLIM (Crespin et al., 2012) over the period 1850–1900 (over the period 1860–1900 in the cases of HadGEM2-CC and HadGEM2-ES).

3 Results and discussion

3.1 Sea-ice changes at 6 ka deduced from observations

Despite the general context of high summer temperatures and low sea-ice conditions characterizing the high northern latitudes during the early to mid-Holocene (Wanner et al., 2008; Polyak et al., 2010; Sundqvist et al., 2010), the quantitative proxy based sea-ice reconstructions based on dynocists display heterogeneous and weak anomalies at 6 ka (Fig. 1). Lower annual mean sea-ice concentration is recorded at the MH in the Fram Strait, northern Baffin Bay and Labrador Sea as compared to PI period. On the contrary, the MH is characterized by higher sea-ice concentration in the Chukchi Sea, and to a lesser extent, in the Barents Sea and in the Barrow Strait (in the CAA).

Most of these dinocyst-based sea-ice records appear directly consistent with local temperature and other sea-ice MH records. In agreement with the reduced ice concentration in Nares Strait and in Fram Strait (id 5 and 17 on Fig. 1), several sea-ice conditions reconstructions based on driftwood deposits and on beach ridges show rare or absent multiyear sea-ice at the MH as far North as the northern coasts of Greenland (Bennike, 2004; Funder and Kjaer, 2007; Funder et al., 2009; Möller et al., 2010; Funder et al., 2011) and Ellesmere Iceland (England et al., 2008), while these coastlines are presently permanently surrounded by pack ice (Polyak et al., 2010). Low sea-ice conditions as compared to the entire Holocene are also inferred from the analysis of IP_{25} in sediment cores collected at the continental slope of West Spitsbergen (Müller et al., 2012).

Further south, along the East Greenland Shelf, Müller et al. (2012) highlighted relatively high sea-ice cover at the MH as compared to the whole Holocene based on IP_{25} and brassicasterol. This contradicts the reconstruction of Jennings et al. (2002) derived from records of ice-rafted detritus, while dinocyst-based reconstruction show no changes at 6 ka as compared to the PI period (id 15). Off northern Iceland, the extent of drift ice seemed to reach a minimum at the MH relative to the past 10 kyr, according to a reconstruction based on the presence of quartz (Andrews et al., 2009).

In the CAA, the MH sea-ice record deduced from various proxies is very heterogeneous which is consistent with the dinocyst-based records (id 3 to 5). On the one hand, the little amount of bowhead bones found indicates high sea-ice coverage (Dyke et al., 1996; Atkinson, 2009) but on the other hand, the analysis of IP_{25} in several sediment cores suggests low spring sea-ice occurrence at the MH compared to the whole Holocene period (Vare et al., 2009; Belt et al., 2010). Further west, the higher sea-ice concentration recorded over the Chukchi Sea at the MH (id 1 and 2) is in agreement with the MH temperature lower than present inferred from oxygen isotope ratios in lake sediments in Alaska (Anderson et al., 2001).

CPD
9, 6515–6549, 2013

Finally, the negative sea-ice concentration anomaly displayed in the Barents Sea (id 18) appears to stand in contrast to continental proxies that show high temperatures at the MH relative to the entire Holocene in the North of Scandinavia, although these latter represent July means (e.g. Seppä and Birks, 2001, 2002). The conclusions derived from the dinocyst-based reconstruction of de Vernal et al. (2013) are thus generally confirmed by other proxy-based reconstructions, even if some discrepancies exist.

3.2 Simulations without data assimilation

We first discuss the simulated sea-ice cover for the model grid points that contain one sea-ice proxy record displayed on Fig. 1. We assume that the spatial representativeness of each core corresponds to the matching grid cell for each model, while the latter have different spatial resolution. We mainly focus on 8 of the 18 available cores (id 1, 2, 3, 4, 5, 15, 17 and 18) because the other ones are located south of the simulated sea-ice edge for most of the GCMs and LOVECLIM for both the MH and the PI periods, and thus display no change in sea-ice concentration. Since the proxy records are calibrated to represent annual means, we primarily focus on the annual means of the models, although seasonal means are also considered in order to get a better understanding of the processes that drive the simulated sea-ice cover.

As compared to the reference period 1850–1900, models results show globally lower annual mean sea-ice concentrations for the MH at the studied locations in the Arctic (Fig. 2). This is consistent with the smaller extent and thinner Arctic sea-ice obtained in models for the MH (Berger et al., 2013). The signal is especially clear over the Chukchi Sea (id 1 and 2) and the CAA (id 3 to 5) where all models depict weak negative anomalies. This annual decrease in sea-ice cover is mainly due to a lower sea-ice concentration in summer in response to the relatively strong increase in insolation (in average $24.35\,\mathrm{W\,m^{-2}}$ for these regions, Fig. 3c). To a lesser extent, fall also contributes to the decrease in annual sea-ice cover especially in the Chukchi Sea, despite a dwindling insolation at 6 ka (in average $-7.27\,\mathrm{W\,m^{-2}}$, Fig. 3d). This can be explained by the inertia of the system: higher summer insolation leads to a decrease in ice thickness and concentration in summer and thus larger oceanic heat fluxes during the following seasons (Manabe and Stouffer, 1980; Renssen et al., 2005; Boé et al., 2009; Crespin et al., 2012). No change in winter and spring sea-ice cover is simulated over the Chukchi Sea and the CAA, these regions being then fully covered by sea-ice and far from the ice edge (Fig. 3a and b).

In the Barents Sea (id 18), the annual mean sea-ice concentration is also lower at the MH compared to the PI period for the majority of the models (Fig. 2). However, the spread is larger than in the Chukchi Sea and two GCMs (CCSM4 and MIROC-ESM) even display positive anomalies. These latter models show higher MH sea-ice concentration all year long with a maximum in spring which is consistent with the decreased insolation during this season ($-2.79\,\mathrm{W\,m^{-2}}$). As for the other models which show negative annual sea-ice concentration anomalies, they have their maximum decrease in sea-ice in fall (CSIRO-Mk3–6-0, MRI-CGCM3, BCC-CSM1–1 and LOVECLIM; Fig. 3d) or in winter (CNRM-CM5, HadGEM2-CC, HadGEM2-ES and MPI-ESM-P; Fig. 3a). This contrasts with the previous situation since the maximum decrease in sea-ice concentration appears delayed compared to the West Arctic and inconsistent with the insolation anomalies during the corresponding season ($-7.92\,\mathrm{W\,m^{-2}}$ in fall and $0.04\,\mathrm{W\,m^{-2}}$ in winter). However, this can easily be explained by the mean state of the models, i.e. the simulated sea-ice concentration in absolute values for PI conditions. In summer, the models cannot melt any sea-ice at the MH compared to PI since most of them depict almost ice-free conditions over the Barents Sea (Fig. 4). The models that have their maximum decrease in sea-ice in fall are the ones that already display a reasonable ice cover during that season for PI, the formation of sea-ice being delayed for MH because of a larger oceanic warming. The other models have a later beginning of the ice season (November–December) for PI, and thus a maximum reduction at that time.

The annual mean simulated MH sea-ice concentration is also lower in Fram Strait (id 17) and in the Greenland Sea (id 15) as compared to the PI values. As in the Barents Sea, the changes in insolation cannot explain alone the simulated sea-ice cover fluctuations as they vary both in timing and in magnitude. Between the models, the simulated mean state likely plays a role there too but the interpretation seems more complex.

As compared to the signal of the proxy-based reconstruction, the simulated sea-ice concentration signal is weaker (the average of all the modelled annual mean anomalies over the studied locations is 3.3 % compared to 6.5 % for the proxy data) and spatially more homogeneous (the average of standard deviations equals 4.5 % compared to 8.8 %). The most noticeable discrepancy between models and data occurs in the Chukchi Sea, where all models simulate a lower sea-ice concentration while the two proxy-based reconstructions show the opposite (Fig. 2). The very heterogeneous sea-ice cover recorded over the CAA is also not reproduced by the models, but this was expected given the complex circulation pattern having local effects on sea-ice (e.g. Lietaer et al., 2008). In the Fram Strait, the sea-ice record agrees with the models mean signal. This is not the case in the Denmark Strait and in the Barents Sea where the mean simulated sea-ice anomalies are negative while the proxy based reconstructions show positive anomalies (Fig. 2), even if some models are able to reproduce the sign and magnitude of the reconstructed signal.

The low skill of the models at the grid scale can be confirmed in a more quantitative way through the calculation of the root mean square error (RMSE) between the results of each climate model and the proxy-based sea-ice reconstructions (ranked in the Fig. 5). Note that this ranking supposedly representing the ability of the climate models in simulating the MH sea-ice concentration should be considered with caution. First, the calculation is performed from the difference between each proxy-based reconstruction and the simulated sea-ice in the corresponding grid cell. This means that a small shift in the spatial structures in the models or small biases in the mean state can lead to large errors. Second, the uncertainty associated to the proxy-based reconstruction, whose value for each location is of the same order of magnitude as the RMSE (Fig. 5), is not taken into account explicitly. Still, this computation of the RMSE displays some interesting features. The models are in better agreement amongst themselves than with the proxy-based reconstructions since the difference in RMSE between any models is smaller (largest difference is equal 5.6 %) than any RMSE using the reconstruction (smallest RMSE is equal to 8.8 %). Furthermore, assuming no change in sea-ice concentration between PI and MH provides an even lower RMSE than the one of any model (this is equivalent to compute the RMSE using a constant field of anomalies being equal to zero for the models results, see the purple bar on Fig. 5). This is consistent with the absence of skill at the local scale discussed in Hargreaves et al. (2013) and in Mairesse et al. (2013) for temperature data.

At a larger scale, the atmospheric circulation changes may explain the spatial structure of the simulated sea-ice anomalies in various models. Here the atmospheric circulation is inferred from the surface pressure for the GCMs because the geopotential heights were not available for all of them at the time of the analysis. For the LOVECLIM simulations, we preferred using the geopotential heights at the pressure level 800 hPa because it is a direct dynamical variable that gives more reliable results than the surface pressure. We have checked for the models for which both the geopotential heights and the surface pressure were available and these two variables give qualitatively the same atmospheric patterns.

The simulated atmospheric circulation changes between the MH and the PI are relatively weak, and appear to have a relatively complex spatial structure (Fig. 6 and 7). Overall, the models disagree on many aspects of the changes, although some common atmospheric patterns can be found in spring (trend similar to a more negative Arctic Oscillation regime), summer and autumn (higher geopotential height over northern Pacific and globally lower over the Eurasian continent) (not shown). Depending on the model selected, the atmospheric circulation can exacerbate or mitigate the decreased sea-ice cover initially due to the higher summer insolation over the Chukchi Sea. Indeed, some models display atmospheric circulation patterns that tend to induce some sea-ice converging towards that region (e.g. CCSM4, MRI-CGCM3, MIROC-ESM) or to push it away (e.g. LOVECLIM no assim, BCC-CSM1-1). Nevertheless, the link between atmospheric circulation and sea-ice concentration is hard to estimate because of the likely dominant role of the thermodynamical response to insolation changes.

CPD
9, 6515–6549, 2013

The role of the atmospheric circulation does not appear to be clearer in the Barents Sea where the positive annual anomalies displayed by CCSM4 and MIROC-ESM cannot be explained by the respectively southerly and easterly winds anomalies simulated there, although the northerly winds simulated by CNRM-CM5 could explain the large negative sea-ice anomalies simulated by this model. The different responses of the models appear thus to imply too many processes to be analyzed in the present framework using available diagnostics. The potential role of atmospheric circulation will be more deeply analyzed in the next section involving data assimilation. In that case, model physics is the same and the only differences are the ones induced by the data constrain which manifests itself in our experiments mainly through atmospheric circulation changes.

3.3 Simulations with data assimilation

Without assimilation, the sea-ice concentration simulated by LOVECLIM is far from the reconstructed one (Fig. 5), especially in the Chukchi Sea where it displays the most negative anomalies among all models while the proxy-based reconstructions show positive ones (Fig. 2). As expected, data assimilation leads to a better agreement with the majority of the proxy-based reconstructions (green triangle to be compared with green squares on Fig. 2). In particular over the Chukchi Sea (id 1 and 2), LOVECLIM with data assimilation has an annual mean ice concentration higher than LOVECLIM without data assimilation by respectively 9.7 % and 12.1 % where the cores 1 and 2 are located. This strong increase is however not sufficient to get positive anomalies. Over that region, the increase of the simulated sea-ice can only occur in summer and autumn because the rest of the year is already fully covered by sea-ice at the MH. However, the significant higher insolation in summer and its lingering effect in autumn prevents any massive increase in sea-ice. Furthermore, the proxy-based reconstruction uncertainty is larger than the signal depicted by the first core, which leads to a too weak constraint to get positive anomalies.

CPD
9, 6515–6549, 2013

Over the CAA (id 3 to 5), the signal of the proxy-based reconstructions is too heterogeneous to be simulated by LOVECLIM. Compared to the simulation without data assimilation, the simulation with data assimilation provides a slightly increased annual mean sea-ice concentration because of a less reduced summer sea-ice. Yet, the annual anomalies are still negative which is consistent with two out of the three cores located there (id 3 and 5). At the Denmark Strait (id 15), the consistency between LOVECLIM and the proxy-based reconstruction is lower after data assimilation, due to a decreased winter and spring sea-ice concentration (Fig. 3a and b). However, the simulated sea-ice stays within the range of the proxy-based reconstruction error.

Further North, in Fram Strait (id 17), LOVECLIM without assimilation is very close to the data and the assimilation has virtually no effect on the simulated sea-ice. Eventually, the simulated annual sea-ice concentration at the Barents Sea (id 18) is increased by 4.8 % in the simulation with data assimilation compared to the simulation without assimilation. LOVECLIM gets this way closer to the data but fails at simulating a positive anomaly to be really consistent with the data that shows an increased sea-ice concentration by 5.7 %. This last proxy-based reconstruction may appear inconsistent with other reconstructions at the MH (see Sect. 3.1). Its trend over the Holocene is more than twice as small as the confidence interval and it is not statistically significative according to the t test (95 % confidence). As it is the only core on the Eurasian coast and is then potentially important, its effect on the whole assimilation process has been tested in additional sensitivity experiments. However, changing its sea-ice concentration value (to 0 and −20 % instead of 5.75 %) does not lead to large changes in sea-ice concentration at the other cores locations or in the RMSE of the model (not shown). This core is thus not critical for the assimilation process at a large scale, LOVECLIM being able to fit locally the new core values without altering significantly the sea-ice results somewhere else.

Overall, the data assimilation leads to a modest decrease of the RMSE (9.6 % compared to 12.8 %, Fig. 5), but the agreement between LOVECLIM with data assimilation and the sea-ice reconstruction is still far from being perfect. This is not surprising

CPD
9, 6515–6549, 2013

considering first the uncertainty of the data which is of the same order of the signal at many locations making the constraint relatively weak. Second, the initial difference between the simulated sea-ice by LOVECLIM without data assimilation and the reconstructed one is large compared to the magnitude of the anomalies. The data assimilation method used here does not consist in changing the physics or parameters of the model but instead in selecting the simulations among an ensemble that best fit the data. Consequently, the potential to modify significantly the way LOVECLIM simulates the sea-ice at the MH is limited. Furthermore, the spatial resolution is rather coarse in LOVECLIM and therefore it cannot take into account small spatial scale processes potentially dominant over regional processes for some records.

The simulation with sea-ice data assimilation is thus not fully consistent with the sea-ice proxy-based reconstruction, but is overall closer to it. The improved consistency associated mainly with higher sea-ice concentration in the Chukchi Sea and in the Barents Sea is achieved through changes in the atmospheric circulation. Indeed, the higher pressure anomaly centered on the Aleutian in the simulation with data assimilation compared to the simulation without data assimilation leads to a cooling in the Chukchi Sea and to a convergence of sea-ice in that region (Fig. 8). On the other side of the Arctic, the lower pressure anomaly centered on Russia is responsible for a cooling over the Barents and thus leads to the increased simulated sea-ice where core 18 is located.

4 Conclusions

We have compared a new quantitative reconstruction of mean annual sea-ice concentration at the MH with models output. Overall, the simulated sea-ice changes at the MH as compared to the PI period are weaker and spatially more homogeneous than the reconstructed ones. As evidenced by the RMSE, the skill of the models at local scale is low and the models are in better agreement between themselves than with data.

CPD
9, 6515–6549, 2013

Sea-ice data assimilation at the mid-Holocene

F. Klein et al.

A general agreement between models and proxy-based reconstructions is found in the Labrador Sea while a large discrepancy occurs in the Chukchi Sea, where models are not able to reproduce the recorded increase in sea-ice concentration at the MH compared to the PI period. Over that region, the increased summer insolation appears to be a dominant driver for the simulated sea-ice changes, while atmospheric circulation can mitigate or exacerbate the decrease in sea-ice concentration. Between Greenland and the Barents Sea, the simulated sea-ice concentration is more variable amongst models making the agreement between models and data depending on the model considered. Over the whole Arctic, but particularly in this regions, the mean state of the models influences the timing of the simulated sea-ice changes with obviously a reduction of the MH sea-ice concentration compared to PI values only at the time when there is already sea-ice in PI.

In addition to the role of insolation and to the link between the mean state and the models response, the mechanisms that control the simulated sea-ice concentration are difficult to precisely identify for all models in the present framework.

When LOVECLIM is constrained to follow the signal recorded in the proxy-based reconstructions using data assimilation, the resulting simulation show overall a better agreement with data. This is mainly due to a decrease in the magnitude of the southerly winds in the Barents Sea and to stronger westerlies in the Beaufort and the Chukchi Seas. The agreement between models results and proxy based reconstructions is, however, still far from perfect. This can be explained to some extent by the relatively small magnitude of the reconstructed signal compared to the uncertainties. The atmospheric circulation anomalies induced by data assimilation can then be viewed as the main process leading qualitatively to a better model-data agreement. A larger amplitude of this pattern would lead to smaller model-data discrepancies but the value obtained in our simulation is setup by the experimental design, in particular the selected data uncertainties.

Acknowledgements. We acknowledge all those involved in producing the PMIP an CMIP multi-model ensemble and all the climate modelling groups for making available their model output.

We acknowledge the World Climate Research Programme's Working Group on Coupled Modelling, which is responsible for CMIP. For CMIP the US Department of Energy's Program for Climate Model Diagnosis and Intercomparison provides coordinating support and led development of software infrastructure in partnership with the Global Organization for Earth System Science Portals. The research leading to these results has received funding from the European Union's Seventh Framework programme (FP7/2007–2013) under grant agreement no. 243908, "Past4Future: Climate change – Learning from the past climate". Computational resources have been provided by the supercomputing facilities of the Université catholique de Louvain (CISM/UCL) and the Consortium des Equipements de Calcul Intensif en Fédération Wallonie Bruxelles (CECI) funded by FRS-FNRS. Hugues Goosse is senior research associate with the FRS/FNRS, Belgium. This is Past4Future contribution XXX.

References

Anderson, L., Abbott, M. B., and Finney, B. P.: Holocene climate inferred from oxygen isotope ratios in lake sediments, Central Brooks Range, Alaska, Quaternary Res., 55, 313–321, doi:10.1006/qres.2001.2219, 2001. 6523

Andrews, J. T., Darby, D., Eberle, D., Jennings, A. E., Moros, M., and Ogilvie, A.: A robust, multisite Holocene history of drift ice off northern Iceland: implications for North Atlantic climate, The Holocene, 19, 71–77, doi:10.1177/0959683608098953, 2009. 6523

Atkinson, N.: A 10 400-year-old bowhead whale (*Balaena mysticetus*) skull from Ellef Ringnes Island, Nunavut: implications for sea-ice conditions in high Arctic Canada at the end of the Last Glaciation, Arctic, 62, 38–44, 2009. 6518, 6523

Belt, S. T., Vare, L. L., Massé, G., Manners, H. R., Price, J. C., MacLachlan, S. E., Andrews, J. T., and Schmidt, S.: Striking similarities in temporal changes to spring sea ice occurrence across the central Canadian Arctic Archipelago over the last 7000 years, Quaternary Sci. Rev., 29, 3489–3504, doi:10.1016/j.quascirev.2010.06.041, 2010. 6523

Bennike, O.: Holocene sea-ice variations in Greenland: onshore evidence, The Holocene, 14, 607–613, doi:10.1191/0959683604hl722rr, 2004. 6523

Berger, A.: Long-term variations of daily insolation and Quaternary climatic changes, J. Atmos. Sci., 35, 2363–2367, 1978. 6517, 6522

Berger, M., Brandefelt, J., and Nilsson, J.: The sensitivity of the Arctic sea ice to orbitally induced insolation changes: a study of the mid-Holocene Paleoclimate Modelling Intercomparison Project 2 and 3 simulations, Clim. Past, 9, 969–982, doi:10.5194/cp-9-969-2013, 2013. 6517, 6518, 6524

Boé, J., Hall, A., and Qu, X.: Current GCM – unrealistic negative feedback in the Arctic, J. Climate, 22, 4682–4695, doi:10.1175/2009JCLI2885.1, 2009. 6525

Braconnot, P., Otto-Bliesner, B., Harrison, S., Joussaume, S., Peterchmitt, J.-Y., Abe-Ouchi, A., Crucifix, M., Driesschaert, E., Fichefet, T., Hewitt, C. D., Kageyama, M., Kitoh, A., Laîné, A., Loutre, M.-F., Marti, O., Merkel, U., Ramstein, G., Valdes, P., Weber, S. L., Yu, Y., and Zhao, Y.: Results of PMIP2 coupled simulations of the Mid-Holocene and Last Glacial Maximum – Part 1: experiments and large-scale features, Clim. Past, 3, 261–277, doi:10.5194/cp-3-261-2007, 2007. 6517

Braconnot, P., Harrison, S. P., Kageyama, M., Bartlein, P. J., Masson-Delmotte, V., Abe-Ouchi, A., Otto-Bliesner, B., and Zhao, Y.: Evaluation of climate models using palaeoclimatic data, Nat. Clim. Change, 2, 417–424, doi:10.1038/nclimate1456, 2012. 6517

Brovkin, V., Bendtsen, J., Claussen, M., Ganopolski, A., Kubatzki, C., Petoukhov, V., and An-dreev, A.: Carbon cycle, vegetation, and climate dynamics in the Holocene: experiments with the CLIMBER-2 model, Global Biogeochem. Cy., 16, 86-1–86-20, doi:10.1029/2001GB001662.1., 2002. 6519

Collins, W. J., Bellouin, N., Doutriaux-Boucher, M., Gedney, N., Halloran, P., Hinton, T., Hughes, J., Jones, C. D., Joshi, M., Liddicoat, S., Martin, G., O'Connor, F., Rae, J., Senior, C., Sitch, S., Totterdell, I., Wiltshire, A., and Woodward, S.: Development and evaluation of an Earth-System model – HadGEM2, Geosci. Model Dev., 4, 1051–1075, doi:10.5194/gmd-4-1051-2011, 2011. 6540

Crespin, E., Goosse, H., Fichefet, T., Mairesse, a., and Sallaz-Damaz, Y.: Arctic climate over the past millennium: annual and seasonal responses to external forcings, The Holocene, 23, 321–329, doi:10.1177/0959683612463095, 2012. 6522, 6525

de Vernal, A. and Rochon, A.: Dinocysts as tracers of sea-surface conditions and sea-ice cover in polar and subpolar environments, IOP Conference Series: Earth and Environmental Science, 14, 012007, doi:10.1088/1755-1315/14/1/012007, 2011. 6521

de Vernal, A., Hillaire-Marcel, C., Rochon, A., Fréchette, B., Henry, M., Solignac, S., and Bonnet, S.: Dinocyst-based reconstructions of sea ice cover concentration during the Holocene

in the Arctic Ocean, the northern North Atlantic Ocean and its adjacent seas, Quaternary Sci. Rev., 79, 111–121, doi:10.1016/j.quascirev.2013.07.006, 2013. 6518, 6521, 6524, 6541
Dubinkina, S., Goosse, H., Sallaz-Damaz, Y., Crespin, E., and Crucifix, M.: Testing a particle filter to reconstruct climate changes over past centuries, Int. J. Bifurcat. Chaos, 1–9, 2011. 6520
Dyke, A. S., Hooper, J., and Savelle, J. M.: A History of Sea Ice in the Canadian Arctic Archipelago based on postglacial remains of the bowhead whale (Balaena mysticetus), Arctic, 49, 235–255, 1996. 6523
Ebert, E. E. and Curry, J. A.: An intermediate one-dimensional thermodynamic sea ice model for investigating ice-atmosphere interactions, J. Geophys. Res., 98, 10085–10109, doi:10.1029/93JC00656, 1993. 6516
England, J. H., Lakeman, T. R., Lemmen, D. S., Bednarski, J. M., Stewart, T. G., and Evans, D. J. A.: A millennial-scale record of Arctic Ocean sea ice variability and the demise of the Ellesmere Island ice shelves, Geophys. Res. Lett., 35, L19502, doi:10.1029/2008GL034470, 2008. 6523
Flückiger, J., Monnin, E., Stauffer, B., Schwander, J., and Stocker, T. F.: High-resolution Holocene N_2O ice core record and its relationship with CH_4 and CO_2, Global Biogeochem. Cy., 16, 10-1–10-8, 2002. 6522
Francis, J. and Vavrus, S. J.: Evidence linking Arctic amplification to extreme weather in mid-latitudes, Geophys. Res. Lett., 39, L06801, doi:10.1029/2012GL051000, 2012. 6517
Funder, S. and Kjaer, K.: Ice free Arctic Ocean, an early Holocene analogue, Eos, Transactions of the American Geophysical Union, Fall Meeting 2007, abstract #PP11A-0203, 2007. 6523
Funder, S., Kjaer, K., Linderson, H., and Olsen, J.: Arctic driftwood – an indicator of multiyear sea ice and transportation routes in the Holocene, Geophys. Res. Abstracts 11 EGU 2009, Vienna, Austria, 2009. 6523
Funder, S., Goosse, H., Jepsen, H., Kaas, E., Kjæ r, K. H., Korsgaard, N. J., Larsen, N. K., Linderson, H., Lyså, A., Möller, P., Olsen, J., and Willerslev, E.: A 10 000-year record of Arctic Ocean sea-ice variability-view from the beach., Science, 333, 747–50, doi:10.1126/science.1202760, 2011. 6517, 6523
Gent, P. R., Danabasoglu, G., Donner, L. J., Holland, M. M., Hunke, E. C., Jayne, S. R., Lawrence, D. M., Neale, R. B., Rasch, P. J., Vertenstein, M., Worley, P. H., Yang, Z.-L., and Zhang, M.: The Community Climate System Model Version 4, J. Climate, 24, 4973–4991, doi:10.1175/2011JCLI4083.1, 2011. 6540

CPD
9, 6515–6549, 2013

Sea-ice data assimilation at the mid-Holocene

F. Klein et al.

Goosse, H. and Fichefet, T.: Importance of ice-ocean interactions for the global ocean circulation: a model study, J. Geophys. Res.-Oc., 104, 23337–23355, 1999. 6516, 6519

Goosse, H., Brovkin, V., Fichefet, T., Haarsma, R., Huybrechts, P., Jongma, J., Mouchet, A., Selten, F., Barriat, P.-Y., Campin, J.-M., Deleersnijder, E., Driesschaert, E., Goelzer, H., Janssens, I., Loutre, M.-F., Morales Maqueda, M. A., Opsteegh, T., Mathieu, P.-P., Munhoven, G., Pettersson, E. J., Renssen, H., Roche, D. M., Schaeffer, M., Tartinville, B., Timmermann, A., and Weber, S. L.: Description of the Earth system model of intermediate complexity LOVECLIM version 1.2, Geosci. Model Dev., 3, 603–633, doi:10.5194/gmd-3-603-2010, 2010. 6519

Goosse, H., Crespin, E., Dubinkina, S., Loutre, M.-F., Mann, M. E., Renssen, H., Sallaz-Damaz, Y., and Shindell, D.: The role of forcing and internal dynamics in explaining the "Medieval Climate Anomaly", Clim. Dynam., 382, 2847–2866, doi:10.1007/s00382-012-1297-0, 2012. 6520

Goosse, H., Roche, D., Mairesse, A., and Berger, M.: Modelling past sea ice changes, Quaternary Sci. Rev., 79, 191–206, doi:10.1016/j.quascirev.2013.03.011, 2013. 6517, 6518

Hargreaves, J. C., Annan, J. D., Ohgaito, R., Paul, A., and Abe-Ouchi, A.: Skill and reliability of climate model ensembles at the Last Glacial Maximum and mid-Holocene, Clim. Past, 9, 811–823, doi:10.5194/cp-9-811-2013, 2013. 6527

Holland, M. M. and Bitz, C. M.: Polar amplification of climate change in coupled models, Clim. Dynam., 21, 221–232, doi:10.1007/s00382-003-0332-6, 2003. 6516

Jennings, A. E., Knudsen, K. L., Hald, M., Hansen, C. V., and Andrews, J. T.: A mid-Holocene shift in Arctic sea-ice variability on the East Greenland Shelf, The Holocene, 12, 49–58, doi:10.1191/0959683602hl519rp, 2002. 6523

Kaufman, D., Ager, T., Anderson, N., Andersond, P., Andrews, J., Bartlein, P., Brubaker, L., Coats, L., Cwynar, L., Duvall, M., Dyke, A., Edwards, M., Eisner, W., Gajewski, K., Geirsdottir, A., Kaplan, M., Kerwin, M., Lozhkin, A., MacDonald, G., Miller, G., Mock, C., Oswald, W., Otto-Bliesner, B., Porinchu, D., Ruhland, K., Smol, J., Steig, E., and Wolfe, B.: Holocene thermal maximum in the western Arctic (0–180° W), Quaternary Sci. Rev., 23, 529–560, doi:10.1016/j.quascirev.2003.09.007, 2004. 6517, 6518

Lietaer, O., Fichefet, T., and Legat, V.: The effects of resolving the Canadian Arctic Archipelago in a finite element sea ice model, Ocean Model., 24, 140–152, doi:10.1016/j.ocemod.2008.06.002, 2008. 6526

CPD
9, 6515–6549, 2013

Sea-ice data assimilation at the mid-Holocene

F. Klein et al.

Lohmann, G. and Gerdes, R.: Sea ice effects on the sensitivity of the thermohaline circulation, J. Climate, 11, 2789–2803, doi:10.1175/1520-0442(1998)011<2789:SIEOTS>2.0.CO;2, 1998. 6516

Mairesse, A., Goosse, H., Mathiot, P., Wanner, H., and Dubinkina, S.: Investigating the consistency between proxy-based reconstructions and climate models using data assimilation: a mid-Holocene case study, Clim. Past, 9, 2741–2757, doi:10.5194/cp-9-2741-2013, 2013. 6520, 6522, 6527

Manabe, S. and Stouffer, R. J.: Sensitivity of a Global Climate Model to an Increase of CO_2 Concentration in the Atmosphere, J. Geophys. Res., 85, 5529–5554, doi:10.1029/JC085iC10p05529, 1980. 6525

Massonnet, F., Fichefet, T., Goosse, H., Bitz, C. M., Philippon-Berthier, G., Holland, M. M., and Barriat, P.-Y.: Constraining projections of summer Arctic sea ice, The Cryosphere, 6, 1383–1394, doi:10.5194/tc-6-1383-2012, 2012. 6517

Mathiot, P., Goosse, H., Crosta, X., Stenni, B., Braida, M., Renssen, H., Van Meerbeeck, C. J., Masson-Delmotte, V., Mairesse, A., and Dubinkina, S.: Using data assimilation to investigate the causes of Southern Hemisphere high latitude cooling from 10 to 8 ka BP, Clim. Past, 9, 887–901, doi:10.5194/cp-9-887-2013, 2013. 6520, 6522

Möller, P., Larsen, N. K., Kjaer, K. H., Funder, S., Schomacker, A., Linge, H., and Fabel, D.: Early to middle Holocene valley glaciations on northernmost Greenland, Quaternary Sci. Rev., 29, 3379–3398, doi:10.1016/j.quascirev.2010.06.044, 2010. 6523

Müller, J., Werner, K., Stein, R., Fahl, K., Moros, M., and Jansen, E.: Holocene cooling culminates in sea ice oscillations in Fram Strait, Quaternary Sci. Rev., 47, 1–14, doi:10.1016/j.quascirev.2012.04.024, 2012. 6517, 6523

Notz, D. and Marotzke, J.: Observations reveal external driver for Arctic sea-ice retreat, Geophys. Res. Lett., 39, 1–6, doi:10.1029/2012GL051094, 2012. 6517

Opsteegh, B. J. D., Haarsma, R. J., Selten, F. M., Kattenberg, A., and Bilt, D.: ECBILT: a dynamic alternative to mixed boundary conditions in ocean models, Tellus A, 50, 348–367, 1998. 6519

Otto-Bliesner, B. L., Joussaume, S., Braconnot, P., Harrison, S. P., and Abe-Ouchi, A.: Modeling and Data Syntheses of Past Climates: Paleoclimate Modelling Intercomparison Project Phase II Workshop, Eos, Transactions American Geophysical Union, 90, Estes Park, Colorado, 2009. 6520

CPD

9, 6515–6549, 2013

Sea-ice data assimilation at the mid-Holocene

F. Klein et al.

Peltier, W.: Global glacial isostasy and the surface of the ice-ahe Earth: the ICE-5G (VM2) Model and GRACE, Annu. Rev. Earth Pl. Sc., 32, 111–149, doi:10.1146/annurev.earth.32.082503.144359, 2004. 6522

Pollard, D. and DeConto, R. M.: Modelling West Antarctic ice sheet growth and collapse through the past five million years, Nature, 458, 329–32, doi:10.1038/nature07809, 2009. 6522

Polyak, L., Alley, R. B., Andrews, J. T., Brigham-Grette, J., Cronin, T. M., Darby, D. A., Dyke, A. S., Fitzpatrick, J. J., Funder, S., Holland, M., Jennings, A. E., Miller, G. H., O'Regan, M., Savelle, J., Serreze, M., St. John, K., White, J. W., and Wolff, E.: History of sea ice in the Arctic, Quaternary Sci. Rev., 29, 1757–1778, doi:10.1016/j.quascirev.2010.02.010, 2010. 6518, 6522, 6523

Renssen, H., Goosse, H., Fichefet, T., Brovkin, V., Driesschaert, E., and Wolk, F.: Simulating the Holocene climate evolution at northern high latitudes using a coupled atmosphere-sea ice-ocean-vegetation model, Clim. Dynam., 24, 23–43, doi:10.1007/s00382-004-0485-y, 2005. 6525

Renssen, H., Seppä, H., Heiri, O., Roche, D. M., Goosse, H., and Fichefet, T.: The spatial and temporal complexity of the Holocene thermal maximum, Nat. Geosci., 2, 411–414, doi:10.1038/ngeo513, 2009. 6517

Rotstayn, L. D., Collier, M. a., Dix, M. R., Feng, Y., Gordon, H. B., O'Farrell, S. P., Smith, I. N., and Syktus, J.: Improved simulation of Australian climate and ENSO-related rainfall variability in a global climate model with an interactive aerosol treatment, Int. J. Climatol., 30, 1067–1088, doi:10.1002/joc.1952, 2009. 6540

Screen, J. a., and Simmonds, I.: The central role of diminishing sea ice in recent Arctic temperature amplification., Nature, 464, 1334–7, doi:10.1038/nature09051, 2010. 6516

Seppä, H., and Birks, H.: July mean temperature and annual precipitation trends during the Holocene in the Fennoscandian tree-line area: pollen-based climate reconstructions, The Holocene, 11, 527–539, doi:10.1191/095968301680223486, 2001. 6524

Seppä, H., and Birks, H.: Holocene climate reconstructions from the Fennoscandian tree-line area based on pollen data from Toskaljavri, Quaternary Res., 57, 191–199, doi:10.1006/qres.2001.2313, 2002. 6524

Serreze, M. C., Barrett, A. P., Stroeve, J. C., Kindig, D. N., and Holland, M. M.: The emergence of surface-based Arctic amplification, The Cryosphere, 3, 11–19, doi:10.5194/tc-3-11-2009, 2009. 6516

Serreze, M. C., Holland, M. M., and Stroeve, J.: Perspectives on the Arctic's shrinking sea-ice cover., Science, 315, 1533–1536, doi:10.1126/science.1139426, 2007. 6517

Stevens, B., Giorgetta, M., Esch, M., Mauritsen, T., Crueger, T., Rast, S., Salzmann, M., Schmidt, H., Bader, J., Block, K., Brokopf, R., Fast, I., Kinne, S., Kornblueh, L., Lohmann, U., Pincus, R., Reichler, T., and Roeckner, E.: The atmospheric component of the MPI-M earth system model: ECHAM6, J. Adv. Model. Earth Syst., 5, 1–27, doi:10.1002/jame.20015, 2013. 6540

Stroeve, J. C., Serreze, M. C., Holland, M. M., Kay, J. E., Malanik, J., and Barrett, A. P.: The Arctic's rapidly shrinking sea ice cover: a research synthesis, Climatic Change, 110, 1005–1027, doi:10.1007/s10584-011-0101-1, 2011. 6516, 6517, 6521

Stroeve, J. C., Kattsov, V., Barrett, A., Serreze, M., Pavlova, T., Holland, M., and Meier, W. N.: Trends in Arctic sea ice extent from CMIP5, CMIP3 and observations, Geophys. Res. Lett., 39, 1–7, doi:10.1029/2012GL052676, 2012. 6517

Sundqvist, H. S., Zhang, Q., Moberg, A., Holmgren, K., Körnich, H., Nilsson, J., and Brattström, G.: Climate change between the mid and late Holocene in northern high latitudes – Part 1: Survey of temperature and precipitation proxy data, Clim. Past, 6, 591–608, doi:10.5194/cp-6-591-2010, 2010. 6517, 6518, 6522

Taylor, K. E., Stouffer, R. J., and Meehl, G. A.: An Overview of CMIP5 and the Experiment Design, B. Am. Meteorol. Soc., 93, 485–498, doi:10.1175/BAMS-D-11-00094.1, 2012. 6520

van Leeuwen, P. J.: Particle Filtering in Geophysical Systems, Mon. Weather Rev., 137, 4089–4114, doi:10.1175/2009MWR2835.1, 2009. 6520

Vare, L. L., Massé, G., Gregory, T. R., Smart, C. W., and Belt, S. T.: Sea ice variations in the central Canadian Arctic Archipelago during the Holocene, Quaternary Sci. Rev., 28, 1354–1366, doi:10.1016/j.quascirev.2009.01.013, 2009. 6518, 6523

Voldoire, A., Sanchez-Gomez, E., Salas y Mélia, D., Decharme, B., Cassou, C., Sénési, S., Valcke, S., Beau, I., Alias, A., Chevallier, M., Déqué, M., Deshayes, J., Douville, H., Fernandez, E., Madec, G., Maisonnave, E., Moine, M.-P., Planton, S., Saint-Martin, D., Szopa, S., Tyteca, S., Alkama, R., Belamari, S., Braun, A., Coquart, L., and Chauvin, F.: The CNRM-CM5.1 global climate model: description and basic evaluation, Clim. Dynam., 40, 2091–2121, doi:10.1007/s00382-011-1259-y, 2012. 6540

Wanner, H., Beer, J., Bütikofer, J., Crowley, T. J., Cubasch, U., Flückiger, J., Goosse, H., Grosjean, M., Joos, F., Kaplan, J. O., Küttel, M., Müller, S. A., Prentice, I. C., Solomina, O., Stocker, T. F., Tarasov, P., Wagner, M., and Widmann, M.: Mid- to

CPD
9, 6515–6549, 2013

Sea-ice data assimilation at the mid-Holocene

F. Klein et al.

Late Holocene climate change: an overview, Quaternary Sci. Rev., 27, 1791–1828, doi:10.1016/j.quascirev.2008.06.013, 2008. 6517, 6522

Watanabe, S., Hajima, T., Sudo, K., Nagashima, T., Takemura, T., Okajima, H., Nozawa, T., Kawase, H., Abe, M., Yokohata, T., Ise, T., Sato, H., Kato, E., Takata, K., Emori, S., and Kawamiya, M.: MIROC-ESM 2010: model description and basic results of CMIP5-20c3m experiments, Geosci. Model Dev., 4, 845–872, doi:10.5194/gmd-4-845-2011, 2011. 6540

Yukimoto, S., Adachi, Y., Hosaka, M., Sakami, T., Yoshimura, H., Hirabara, M., Tanaka, T. Y., Shindo, E., Tsujino, H., Deushi, M., Mizuta, R., Yabu, S., Obata, A., Nakano, H., Koshiro, T., Ose, T., and Kitoh, A.: A new global climate model of the meteorological research institute: MRI-CGCM3 – model description and basic performance, J. Meteorol. Soc. Jpn. A, 90, 23–64, doi:10.2151/jmsj.2012-A02, 2012. 6540

Zhang, J., Woodgate, R., and Moritz, R.: Sea ice response to atmospheric and oceanic forcing in the Bering Sea, J. Phys. Oceanogr., 40, 1729–1747, doi:10.1175/2010JPO4323.1, 2010. 6517

CPD

9, 6515–6549, 2013

Sea-ice data assimilation at the mid-Holocene

F. Klein et al.

Table 1. CMIP5/PMIP3 GCMs characteristics and references.

Model name	Modelling center	Reference
BCC-CSM1-1	Beijing Climate Center, China Meteorological Administration	http://bcc.cma.gov.cn/bcccsm/
CCSM4	National Center for Atmospheric Research	Gent et al. (2011)
CNRM-CM5	Centre National de Recherches Meteorologiques/Centre Europeen de Recherche et Formation Avancees en Calcul Scientifique	Voldoire et al. (2012)
CSIRO-Mk3.6.0	Commonwealth Scientific and Industrial Research Organization in collaboration with Queensland Climate Change Centre of Excellence	Rotstayn et al. (2009)
HadGEM2-CC	Met Office Hadley Centre	Collins et al. (2011)
HadGEM2-ES	Met Office Hadley Centre	Collins et al. (2011)
MIROC-ESM	Japan Agency for Marine-Earth Science and Technology, Atmosphere and Ocean Research Institute (The University of Tokyo), and National Institute for Environmental	Watanabe et al. (2011)
MPI-ESM-P	Max Planck Institute for Meteorology	Stevens et al. (2013)
MRI-CGCM3	Meteorological Research Institute	Yukimoto et al. (2012)

CPD
9, 6515–6549, 2013

Table 2. Description of all the cores available in 6 ± 0.5 ka (-4050 ± 0.5 kyr AD) used to reconstruct sea-ice cover (de Vernal et al., 2013). The table shows the cores id used in this study, their name, location, latitude, longitude and the reconstructed sea-ice concentration anomalies (reference period 1850–1900 AD).

Id	Core name	Location	Lat	Lon	6k sic ano (%)
1.	HLY05JPC	Chukchi Sea	72.69	−157.52	8.95
2.	GGC19	Chukchi Sea	72.16	−155.51	22.60
3.	LS009	Lancaster Sound	74.19	−81.195	−4.49
4.	BS004	Barrow Strait	74.27	−91.09	12.60
5.	HU008	Nares Strait	77.27	−74.32	−14.53
6.	HU021TWC	Labrador Sea	58.37	−57.51	−5.82
7.	HU013	Labrador Sea	58.21	−48.31	−12.59
8.	MD2227	Atlantic	58.21	−48.37	−5.08
9.	HU044	East Canadian margin	44.49	−55.19	0.14
10.	MD2033	Gulf of St Lawrence	44.66	−55.62	−0.52
11.	HU094	Atlantic	50.2	−45.69	−8.25
12.	HU085	Atlantic	53.98	−38.64	−1.85
13.	MD2254	Atlantic	56.8	−30.66	3.53
14.	HM025	Faroe-Shetland Chan.	60.11	−6.07	1.61
15.	JM1207	Denmark Strait	68.1	−29.35	0.88
16.	M23323	Norwegian Sea	67.77	5.92	2.07
17.	MSM712	Fram Strait	78.92	6.77	−5.45
18.	PL112	Barents Sea	71.27	42.61	5.75

CPD
9, 6515–6549, 2013

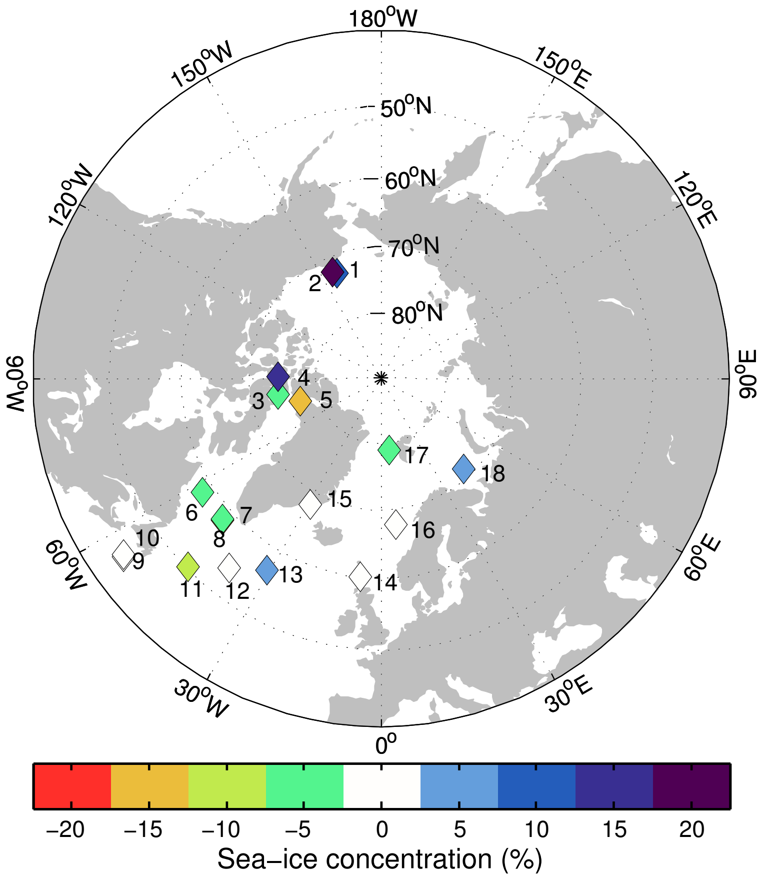

Fig. 1. Proxy-based annual mean sea-ice concentration anomalies (in %) at the MH (reference period 1850–1900 AD).

CPD
9, 6515–6549, 2013

Sea-ice data assimilation at the mid-Holocene

F. Klein et al.

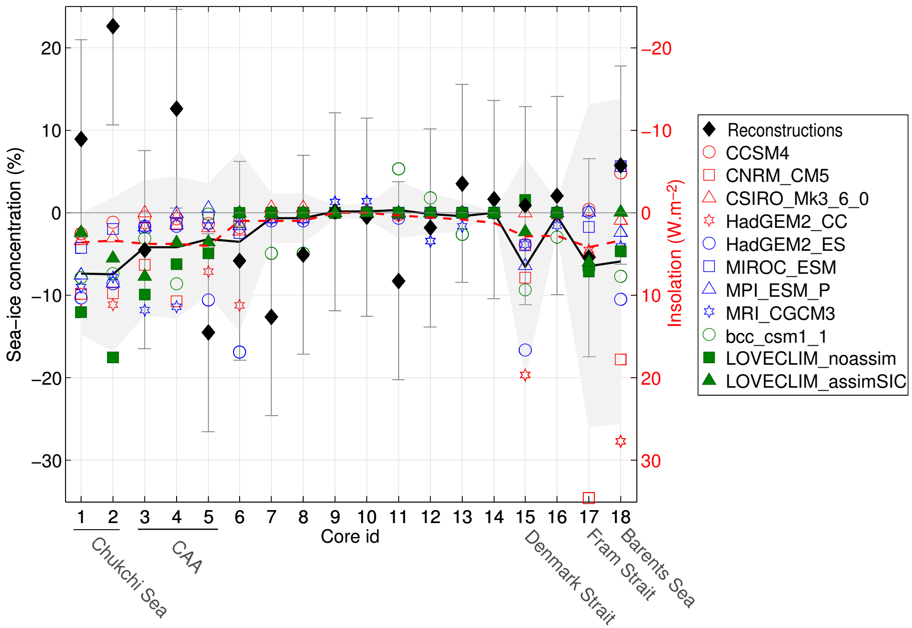

Fig. 2. Mid-Holocene annual mean sea-ice concentration anomalies (in %) for the proxy-based reconstructions (black diamonds with error bars) and the corresponding climate models results. The thick black line is the models mean. The grey shaded areas is the models mean ±2 standard deviations. The dashed red line represents the annual mean insolation at each studied location (in $\mathrm{W\,m^{-2}}$) and corresponds to the reversed right axis. The reference period is 1850–1900 AD.

CPD

9, 6515–6549, 2013

Sea-ice data assimilation at the mid-Holocene

F. Klein et al.

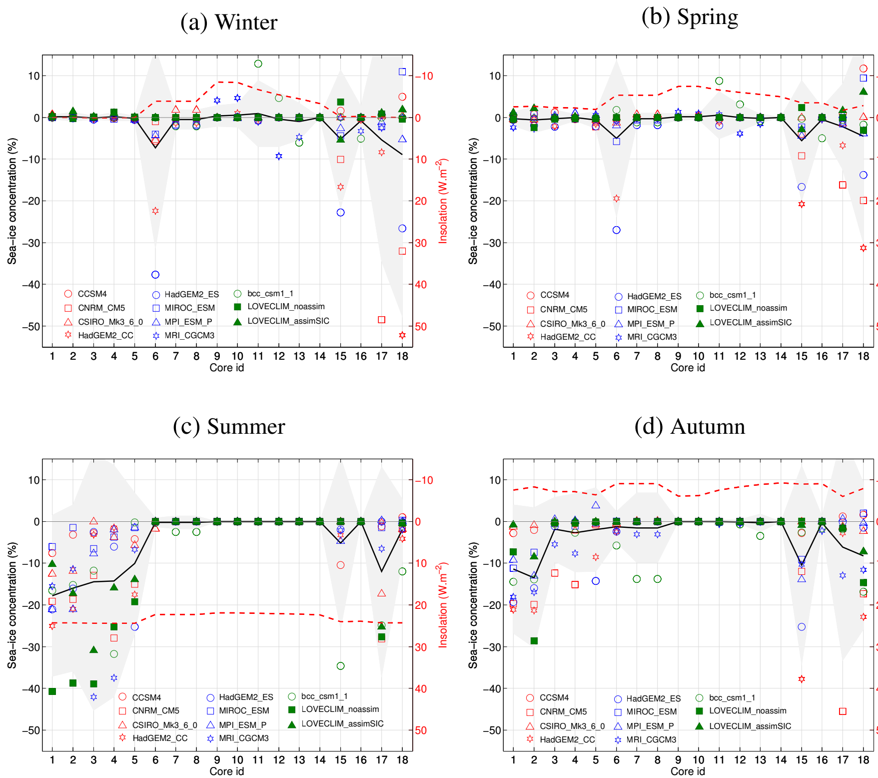

Fig. 3. Mid-Holocene seasonal mean sea-ice concentration anomalies (in %) for the climate models results corresponding to the cores locations. The thick black line corresponds to the models mean. The grey shaded areas is the models mean ±2 standard deviations. The dashed red line represents the seasonal mean insolation at each studied location (in W m^{-2}) and corresponds to the reversed right axis. The reference period is 1850–1900.

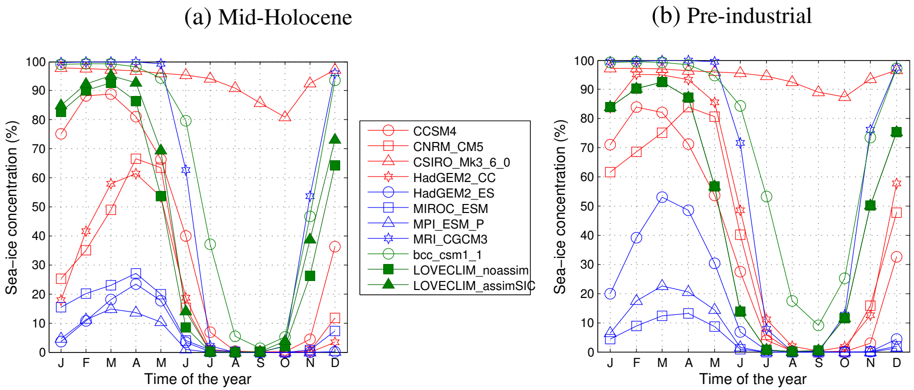

Fig. 4. Mid-Holocene (6 ka) and pre-industrial (1850–1900 AD) mean seasonal cycles of sea-ice concentration (in %) in the Barents Sea (id 18).

CPD
9, 6515–6549, 2013

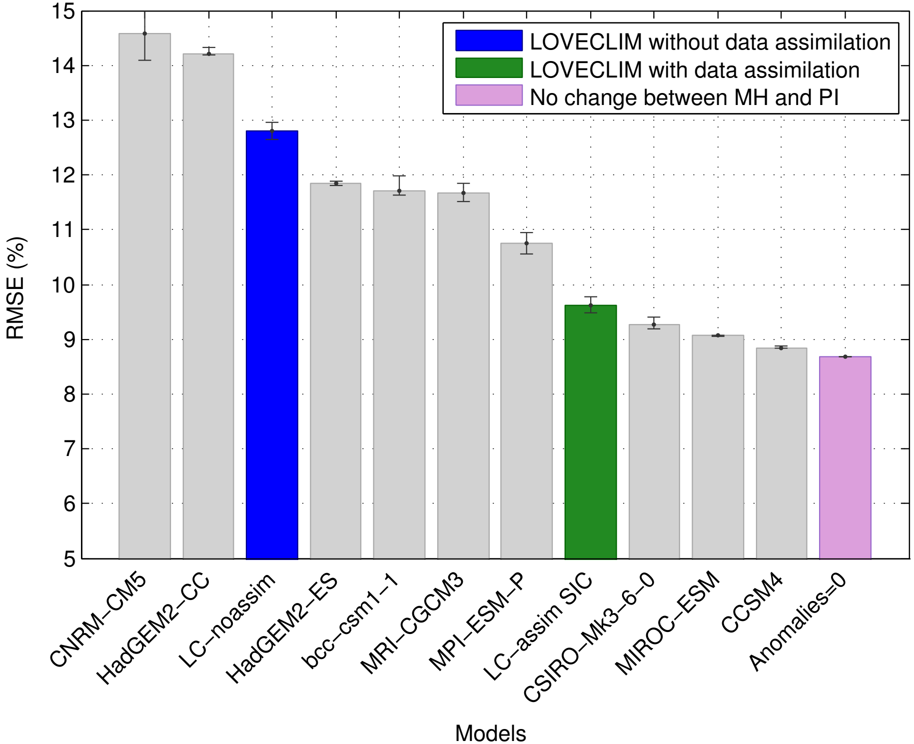

Fig. 5. Ranked RMSE between the MH sea-ice anomalies (reference period 1850–1900 AD) simulated by each model and the proxy based reconstructions. The error bars correspond to the range of the RMSE when changing the reference period to 1850–1875 AD and 1875–1900 AD. The purple bar is the RMSE computed assuming no change between MH and PI.

CPD
9, 6515–6549, 2013

Sea-ice data assimilation at the mid-Holocene

F. Klein et al.

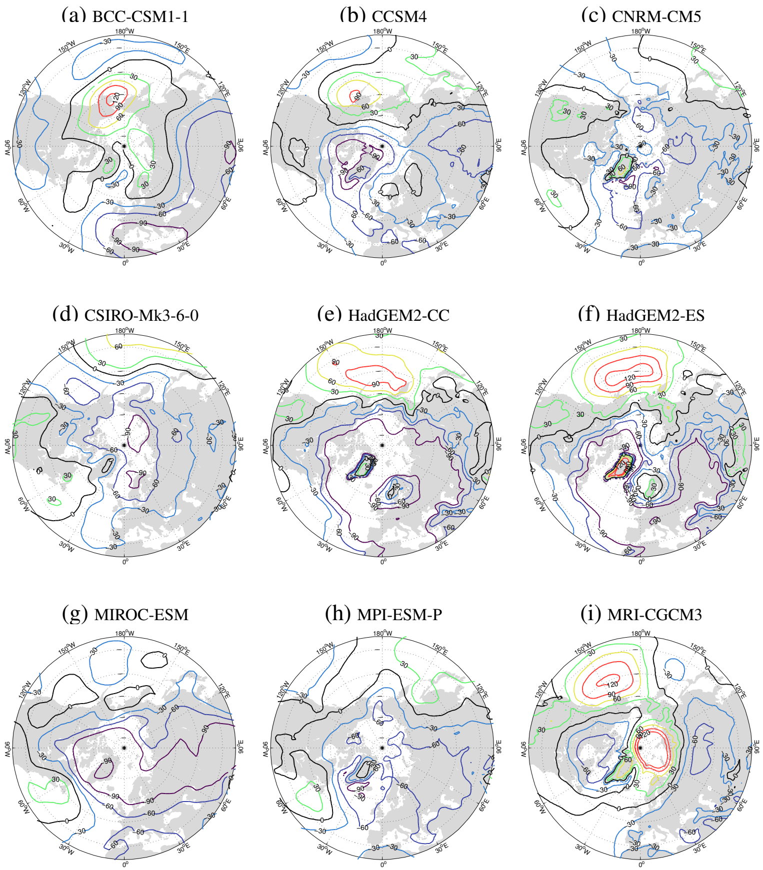

Fig. 6. Annual mean surface pressure anomalies (in Pa) simulated by the GCMs for the MH (reference period 1850–1900 AD).

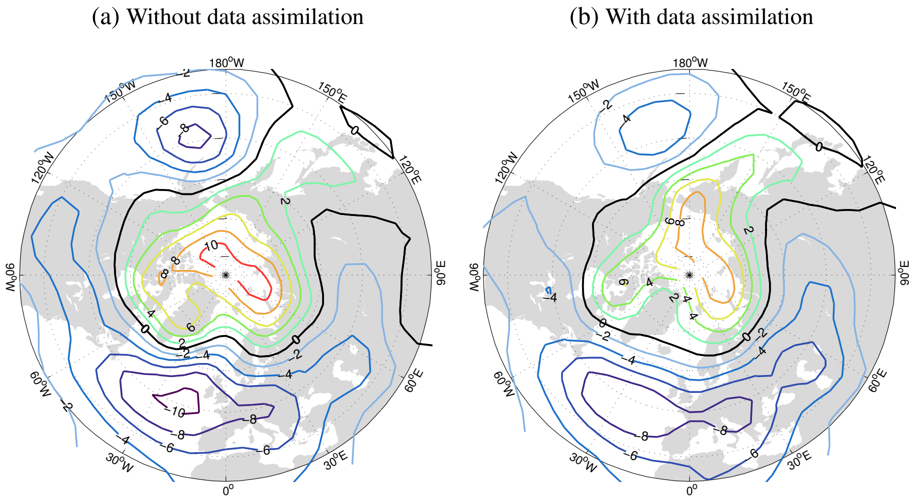

Fig. 7. MH annual geopotential height anomalies (in m) at 800 hPa simulated by **(a)** LOVECLIM without assimilation and **(b)** LOVECLIM with assimilation of sea-ice proxy data. The reference period is 1850–1900 AD.

CPD
9, 6515–6549, 2013

Title Page
Abstract | Introduction
Conclusions | References
Tables | Figures
◀I | ▶I
◀ | ▶
Back | Close
Full Screen / Esc
Printer-friendly Version
Interactive Discussion

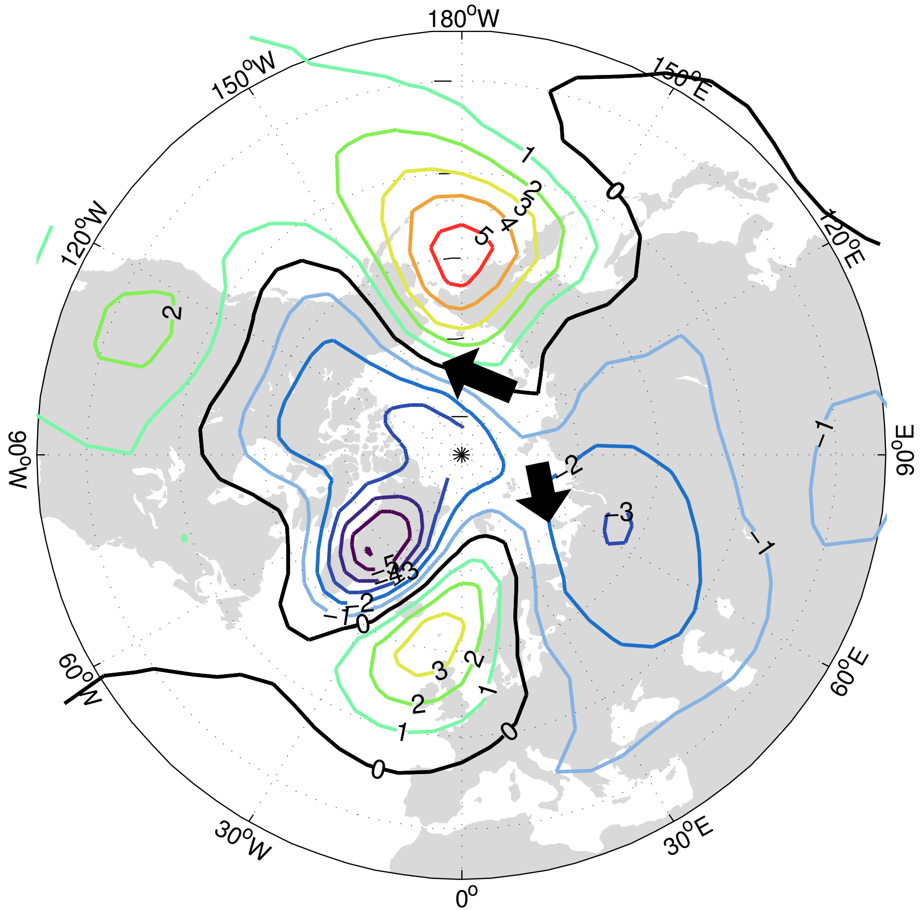

Fig. 8. Difference between the geopotential height anomalies (in m) at 800 hPa of LOVECLIM with sea-ice data assimilation and LOVECLIM without data assimilation. The black arrows show the flow responsible for the change in sea-ice at the Barents Sea and the Chukchi Sea.

CPD
9, 6515–6549, 2013

Sea-ice data assimilation at the mid-Holocene

F. Klein et al.

Title Page
Abstract | Introduction
Conclusions | References
Tables | Figures
◀| |▶
◀ ▶
Back | Close
Full Screen / Esc
Printer-friendly Version
Interactive Discussion